Reevaluation of total-column ozone trends and of the Effective Radiative Forcing of ozone-depleting substances

Olaf Morgenstern[1], Stacey M. Frith[2], Gregory E. Bodeker[3], Vitali Fioletov[4], and Ronald J. van der A[5]

[1]National Institute of Water and Atmospheric Research (NIWA), Wellington, New Zealand
[2]NASA System Science and Applications, Lanham, MD, USA
[3]Bodeker Scientific, Alexandra, New Zealand
[4]Environment Canada, Downsview, ON, Canada
[5]KNMI, De Bilt, Netherlands

Key Points:

- We evaluate total-column ozone trends for 1979-2000 and 1997-2020.
- For 1997-2020 we find significant global- and Southern-Hemisphere mean positive trends.
- The Effective Radiative Forcing of ozone-depleting substances is now more consistent with two previous evaluations.

Corresponding author: Olaf Morgenstern, olaf.morgenstern@niwa.co.nz

Abstract

We evaluate total-column ozone trends using a piecewise linear regression approach and maximizing usage of five gridded total-column ozone datasets. The new approach yields more consistent estimates of observed ozone loss during 1979-2000, when halocarbon concentrations were increasing, and consequently, using CMIP6 simulations, an increased Effective Radiative Forcing estimate of ozone-depleting substances with a substantially reduced uncertainty range versus an earlier evaluation. At more than 84% confidence it is now larger than zero and compares more favorably with two previous evaluations. We furthermore find significant, positive post-1997 global- and Southern-Hemisphere mean trends, respectively, in these four datasets. For the extrapolar region (60°S-60°N) and for the Northern Hemisphere, the assessment whether there is a positive trend is inconclusive and depends on which observational dataset is included in the calculation.

Plain Language Summary

Changes in overhead ozone amounts reflect the impact of the Montreal Protocol, designed to protect the ozone layer, but also several other influences. Here we assess five different ozone datasets using satellite and ground-based observations as well as fields generated by present-generation climate models. For the period 1979-2000, during which stratospheric ozone depletion got established, we find good agreement for the whole globe and for selected sub-regions across the observational datasets. For 1997-2020, in the global- and Southern-Hemisphere means we find a significant, positive ozone trend. For a region excluding both poles and for the Northern Hemisphere the uncertainty range still includes zero. Using observational and model results for 1979-2000 we recalculate the impact of ozone-depleting substances accounting for ozone depletion on the Earth' radiation balance. We find a slightly larger net impact than a previous evaluation, which within the uncertainty bounds is much more likely to be positive and is more consistent with two previous evaluations.

1 Introduction

Halocarbons are amongst the larger drivers of anthropogenic climate change, ranking behind CO_2 and CH_4 and about on par with N_2O for their direct radiative forcing (Myhre et al., 2013). Here, direct radiative forcing only accounts for the heat-trapping properties of these greenhouse gases, discounting any impacts on the radiation balance due to chemical or other feedbacks, with the exception of a stratospheric temperature adjustment (Forster et al., 2016). However, in the case of the halocarbons, ozone depletion provides an important offsetting contribution due to its cooling impact on climate. Earlier efforts to quantify the Effective Radiative Forcing (ERF, which now does account for atmospheric adjustments such as chemical ozone depletion) of halocarbons, or equivalently the radiative forcing associated with the ozone depletion itself, were either limited by disagreements and uncertainty about the magnitude of modelled and observed ozone depletion or relied on very few models, meaning model uncertainty was not well accounted for (Søvde et al., 2011; Shindell et al., 2013). Morgenstern et al. (2020) offered a path forward to quantify their ERF despite the large model disagreements which remain amongst six interactive-chemistry models available in the CMIP6 ensemble. However, their approach, an emergent-constraint technique projecting modelled and observed ozone trends onto the associated ERF, is affected both by significant disagreements in the 1979-2000 ozone trends between three underlying observational ozone climatologies used in their analysis, as well as by the statistical uncertainties of those trends themselves. Their approach relied on only 18 years each of observational and model data covering 1979-2000, with four years during this period excluded from the analysis due to a substantial volcanic influence. Furthermore, for high-latitude observations of total-column ozone (TCO), they took a minimalistic approach, rejecting all data points representing

polar winter unless covered by all three climatologies. Here we complement their method with a related approach maximally using four gridded observational TCO datasets and assess the impact this complementary method has on the best estimates and the uncertainty ranges of ozone trends and the ERF of halocarbons, respectively.

The 2018 World Meteorological Organization Scientific Assessment of Ozone Depletion (Braesicke et al., 2018) found 1997-2016 trends of extrapolar-mean TCO to be insignificant. We will reevaluate this finding using data up to the year 2020.

2 Observational data and models

Models and observational climatologies are similar to those used by Morgenstern et al. (2020), except for the SBUV v86 ozone climatology (Frith et al., 2014) omitted by Morgenstern et al. (2020) because unlike the other climatologies it does not cover the poles in any season. We also include here the World Ozone and Ultraviolet Data Center's groundbased TCO dataset as it provides a long-term reference dataset not reliant on satellite data. The models, CMIP6 simulations, TCO observational climatologies, and key references are listed in Tables 1 and S1 in the supplement.

Dataset	Coverage	Resolution	Reference
WOUDC ground-based	1964-2020	Zonal-mean, 5°	Fioletov et al. (2002)
SBUV v8.6	1970-2020	Zonal mean, 5°	Frith et al. (2014)
NIWA-BS (v3.4, unpatched)	1978-2016	1.25° × 1°	Bodeker et al. (2020)
NIWA-BS (v3.5.1, unpatched)	1978-2019	1.25° × 1°	Bodeker and Kremser (2021)
MSR-2	1979-2020	0.5° × 0.5°	van der A et al. (2015)
	1970-1978	1.5° × 1°	

Table 1. Five observational TCO climatologies and the reference ozone field used to force CMIP6 models without interactive ozone.

3 Method

Linear fits to observational time series subject to meteorological noise usually produce the largest uncertainties at both end points of the data to be fitted. However, if data exist outside the period of interest, these data can be used in a generalized fitting process using piecewise linear regression, better constraining the end points of the fit and thus reducing the uncertainty in the estimated trend. This is the central idea informing this re-assessment of TCO trends and the ERF of halocarbons. Three of the four node years that need to be used here are straightforwardly identified: 1970 marks the start of any space-based observations of TCO. In late 1978 the Total Ozone Mapping Spectrometer (TOMS) satellite instrument became operational, meaning from 1979 onwards space-based observations are more consistent than previously. 2020 marks the end point of three of the climatologies used here. Around the turn of the century, halogen loading in the stratosphere started to decrease. We will variously use two different central nodes around this time: The year 1997 marks the actual turnaround in halogens, and Weber et al. (2018) and Braesicke et al. (2018) give extrapolar ozone trends for 1997-2016. Morgenstern et al. (2020) use TCO between 1979 and 2000. For purposes of evaluating TCO trends during the period of increasing ODSs, this extended period produces smaller uncertainties for the resultant trend than having a node in 1997. We will thus state ozone trends for 1979-2000, to capture observational ozone loss, and 1997-2016 and 1997-2020, respectively.

Below we outline the steps taken to bring the four observational and five modelled TCO fields, and the ozone climatology used in the CMIP6 experiments, onto a common grid and coverage, with optimal usage of observational data.

1. All data (observational and modelled, "historical" merged with 'future' TCO datasets following the Shared Socio-Economic Pathway (SSP) 2-4.5 (Riahi et al., 2017)) are interpolated to the same 0.5° latitudinal grid as zonal means.
2. For the period 1970-2020, polar and other data gaps in the observational ozone climatologies (table 1) are filled as much as possible, using firstly MSR-2 and secondly SBUV v86 data. Details of this process are discussed in the Supplement. After this step, data gaps are now restricted to latitudes and times with neither MSR-2 nor SBUV v86 data.
3. We fill most remaining data gaps (which are almost all in the period 1970-1978) using a regression fit accounting for equivalent effective stratospheric chlorine (EESC Newman et al., 2007) and equivalent CO_2 (Morgenstern, 2021). Data generated in this way are only used for purposes of error analysis, not in the calculation of best-estimate linear trends. Remaining data gaps after this step are three two-year gaps as discussed above and small repetitive data gaps during Antarctic winter (supplement, figure S1).

In comparison to the method used by Morgenstern et al. (2020), the above process differs in two key respects: A more complete usage of available data, both in the spatial dimension, with much smaller polar data gaps remaining, and in the temporal dimension, with data usage extended from 1979-2000 to 1970-2020. A further difference is that we additionally use the SBUV v86 and the WOUDC ground-based climatologies and also consider a more recent version of NIWA-BS. Unlike Morgenstern et al. (2020) we do not however use TOMS-SBUV (Stolarski & Frith, 2006) which is considered superseded.

4 Results

4.1 TCO trends using the expanded datasets

Figure 1 shows the familiar widespread extratropical ozone loss in the period 1979-2000, with losses maximizing in both polar regions during spring. However, the figure also indicates ozone loss, albeit mostly insignificant at 97.5% confidence, during the 1970s as measured by SBUV and ground-based instruments, qualitatively consistent with model studies that suggest significant ozone depletion in this period (Langematz et al., 2016). Furthermore, for 1997-2020 there are some significant positive TCO trends at southern high latitudes, e.g. 1.7 ± 1.3 DU a^{-1} (95% confidence) at South Pole in spring, similar to the references quoted by Langematz et al. (2018) (their table 4-1) for various more restricted periods. High-confidence trends, by the measure used here, are mostly restricted to the ozone hole region and season.

Also noteworthy are continuing ozone decreases during autumn and winter in the Arctic of up to about -0.5 to -1 DU a^{-1}. These are generally insignificant in the multi-observational mean; it remains to be seen whether this is a statistical anomaly or whether systematic driving factors, such as continuing cooling of the stratosphere due to increasing greenhouse gases or any trends in the Brewer-Dobson Circulation, may contribute to this feature.

Figure 2 shows annual- and regional-mean trends as found here. The top panel is comparable to Morgenstern et al. (2020) in that it uses the same type of simple linear fit. Replacing TOMS-SBUV with SBUV v86 and the ground-based dataset has clearly improved the consistency across four of the datasets. NIWA-BS v3.5.1 has an anomalous long-term drift versus the four other observational datasets of nearly 0.2 DU/year

(versus GB, not shown) in the global mean and therefore not included in calculating the MOM. Reverting to 4NPLR results in a decrease in the trends (indicating that a node in the year 2000 is not optimal, as noted above), but the longer interval (1979-2000) results in reduced uncertainties in the trend over this period versus the simple linear regression, and also versus any shorter periods such as 1979-1997. This applies to all four sub-regions studied. The SBUV, ground-based, and MSR-2 records are in good agreement.

Trends for 1997-2020 are positive in all cases, exceeding 97.5% confidence for four global and four Southern-Hemisphere means. For the extrapolar (60°S-60°N) mean, the trends are significant at 84% confidence for all five observational datasets and at 97.5% confidence for three of them. Trends in the SBUV and NIWA-BS v3.4 records do not meet the 97.5% confidence threshold – in the case of NIWA-BS, narrowly. However, the MSR-2 and ground-based climatologies, which have not received any fill-in for this period and latitude band (figure 1), have positive trends at very high confidence levels (table 2). The disagreements between the datasets mean that the multi-observational mean trend (excluding NIWA-BS v3.5.1) is also narrowly not significant at 97.5% confidence. Our findings imply that the assessment that the 1997-2016 extrapolar TCO trend is insignificant (Braesicke et al., 2018), extended to cover 1997-2020, now depends on which dataset is included in the calculation. Conducting a simple linear fit to 1997 to 2016 data yields insignificant trends at 97.5% confidence for four climatologies and the multi-observational mean (MOM), i.e. our results are consistent with Braesicke et al. (2018). The reduction in uncertainty for 1997-2020 is in roughly equal parts due to four more years of data available versus Braesicke et al. (2018) and to using piecewise linear regression replacing a simple linear fit here (not shown). For the Northern Hemisphere, confidence that TCO is increasing over 1997-2020 is less than 97.5% for three of the climatologies. Here the positive TCO trend has not unambiguously emerged from the climatological noise.

4.2 Cause of the improved consistency across observational datasets

Next we assess how much individual differences versus the method used by Morgenstern et al. (2020) contribute to the improved agreement of the 1979-2000 trends (table 2). Here the error in the MOM is estimated as

$$\epsilon_{MOM} = \sqrt{\max \epsilon_k^2 + \mu^2}, \tag{1}$$

where ϵ_k are the 68% (1σ) uncertainties of the individual observational trends and μ is the standard deviation of the best-estimate trends.

This analysis shows that only filling in polar and other data gaps in the period 1979-2000 (step 1) in absolute terms leads to an increase in both the TCO trends and in the associated statistical errors relative to Morgenstern et al. (2020)'s results due to a better coverage of the polar regions subject to both larger trends and larger meteorological variability. However, replacing the TOMS-SBUV climatology with SBUV and WOUDC has helped improve the consistency across four of the datasets. NIWA-BS 3.5.1 drifts versus NIWA-BS 3.4 and the other datasets, with trends in both periods (1979-2000 and 1997-2020) larger than in the other datasets. Bringing in an additional 20 years of data and now conducting a three-node piecewise linear regression (step 2) lead to a reduction of 1979-2000 trends by 0.12 DU a^{-1} on average, good consistency of the trends derived from the climatologies, and reduced statistical uncertainties from 0.09 to 0.07 DU a^{-1}. Additionally bringing in the data for 1970-1978 slightly further reduces the mean trends but leads to an increase of the statistical uncertainties. In Morgenstern et al. (2020)'s calculation, the trend disagreement μ noticeably affects the overall uncertainty of TCO trends, whereas it is negligible in most situations considered here so long as NIWA-BS v3.5.1 is not included in the calculation.

Climatology	Step 1 90°S-90°N	Step 2 90°S-90°N	Step 3 90°S-90°N	1997-2020 60°S-60°N	1997-2016 60°S-60°N
SBUV v86	-0.64 ± 0.09	-0.49 ± 0.07	-0.47 ± 0.08	0.05 ± 0.05	0.00 ± 0.07
NIWA-BS v3.4	-0.61 ± 0.09	-0.51 ± 0.07	-0.48 ± 0.08	0.10 ± 0.05	0.00 ± 0.08
NIWA-BS v3.5.1	-0.48 ± 0.08	-0.36 ± 0.07	-0.34 ± 0.08	0.27 ± 0.05	0.30 ± 0.06
WOUDC ground-based	-0.60 ± 0.09	-0.48 ± 0.07	-0.47 ± 0.08	0.14 ± 0.05	0.05 ± 0.07
MSR-2	-0.60 ± 0.09	-0.46 ± 0.07	-0.43 ± 0.08	0.15 ± 0.05	0.10 ± 0.08
MOM	-0.61 ± 0.09	-0.49 ± 0.07	-0.46 ± 0.08	0.11 ± 0.07	0.04 ± 0.09

Table 2. TCO trends from the observational estimates. Left to right: using simple linear regression over 1979-2000 with data gaps filled (step 1), using three-node piecewise linear regression over the period 1979-2020, with nodes in 1979, 2000, and 2020 (step 2), using four-node piecewise linear regression over the period 1970-2020, with nodes in 1970, 1979, 2000, and 2020 (step 3). Rightmost two columns: Trends for 60°S-60°N for 1997-2020 derived using 4NPLR with central nodes with nodes in 1970, 1979, 1997, and 2020. Trends for 1997-2016 are for simple linear regression (i.e. two nodes in 1997 and 2016). Uncertainties refer to the 68% confidence level. The MOM does not include NIWA-BS 3.5.1.

In all, it becomes clear that deriving 1979-2000 TCO trends using three-node piecewise linear regression based on the extended period 1979-2020 yields consistent trend estimates subject to relatively smaller uncertainties than a simpler approach ignoring the later data.

5 Using the improved TCO trends in the calculation of the ERF of ozone-depleting substances

We here repeat Morgenstern et al. (2020)'s calculation of the Effective Radiative Forcing of ODSs, this time using TCO trends derived for 1979-2000 using 3NPLR with nodes in 1979, 2000, and 2020. The calculation shows that now the 68% confidence interval for the ERF of ODSs of 0.085 ± 0.059 Wm^{-2} (relative to the observational-mean ozone climatology) no longer includes zero, and the probability that the ERF is negative for the mean ozone climatology is now 7% (with a range of 3 to 11% for the four ozone climatologies), not 24% as found by Morgenstern et al. (2020). In IPCC uncertainty language (Mastrandrea et al., 2011), this makes it "very likely" that the ERF is positive. The result is also in better agreement with two earlier evaluations of 0.08 (Søvde et al., 2011) and 0.13 ± 0.07 Wm^{-2} (Shindell et al., 2013), but remains notably smaller than the forcing of 0.18 ± 0.15 Wm^{-2} assessed by Myhre et al. (2013).

6 Discussion and conclusions

There are no specific errors in the calculation by Morgenstern et al. (2020), but it is obvious that two factors contributed to inflated uncertainties in their calculation. Firstly they used an outdated TCO climatology (TOMS-SBUV) as one of three reference datasets with a slightly anomalous TCO trend in 1979-2000. Secondly, their restrictive usage of available TCO data inflated uncertainties in trend estimates. A relatively small modification in their methodology, namely replacing ozone trends derived using simple linear regression with piecewise linear regression, making maximum use of five available observational TCO climatologies, reduces uncertainty ranges of assessed trends. This makes the observational ozone climatologies more useful as "emergent constraints", yielding thus

a more robust estimate of the ERF of ozone-depleting substances. Our best-estimate ERF of ODSs (0.085 Wm^{-2}) is slightly larger than Morgenstern et al. (2020)'s estimate, although it is comfortably within the error bounds. This increase makes the new estimate more consistent with two earlier evaluations, but the central estimate by Myhre et al. (2013) of 0.18 Wm^{-2} remains unlikely to be consistent with ours.

The analysis finds significant positive global-, and Southern-Hemisphere mean trends in some observational TCO observational gridded TCO datasets for 1997-2020. The extrapolar-mean trend has not fully emerged in all observational datasets at high confidence. Latitudinally and seasonally resolved trends for 1997-2020, which are subject to larger meteorological noise than meridional and annual averages, are only significant seasonally in the southern polar region.

Acknowledgments

OM was supported by the NZ Government's Strategic Science Investment Fund (SSIF) through the NIWA programme CACV. GEB acknowledges funding by the Deep South National Science Challenge (`https://deepsouthchallenge.co.nz`), an initiative of the New Zealand Ministry of Business, Innovation, and Employment. We acknowledge the World Climate Research Programme, which, through its Working Group on Coupled Modelling, coordinated and promoted CMIP6. We thank the climate modeling groups for producing and making available their model output, the Earth System Grid Federation (ESGF) for archiving the data and providing access, and the multiple funding agencies who support CMIP6 and ESGF. Scripts and intermediate data used in the calculations and graphics presented here can be downloaded at `https://zenodo.org/record/5118284`. This material includes the updated observational ozone climatologies, the later years of some of which are not in the public domain yet. CMIP6 simulation data can be downloaded at `https://esgf-node.llnl.gov/search/cmip6/`. TCO data used here have been ensemble-averaged using the 'ncea' command. Top-of-atmosphere radiation fluxes needed in the calculation of the ERF of ODSs are derived by Morgenstern et al. (2020).

References

Bodeker, G. E., & Kremser, S. (2021). Indicators of Antarctic ozone depletion: 1979 to 2019. *Atmospheric Chemistry and Physics*, *21*(7), 5289–5300. Retrieved from `https://acp.copernicus.org/articles/21/5289/2021/` doi: 10.5194/acp-21-5289-2021

Bodeker, G. E., Nitzbon, J., Tradowsky, J. S., Kremser, S., Schwertheim, A., & Lewis, J. (2020). A global total column ozone climate data record. *Earth System Science Data Discussions*, *2020*, 1–33. Retrieved from `https://essd.copernicus.org/preprints/essd-2020-218/` doi: 10.5194/essd-2020-218

Braesicke, P., Neu, J., Fioletov, V., Godin-Beekmann, S., Hubert, D., Petropavlovskikh, I., ... Sinnhuber, B.-M. (2018). Update on global ozone: Past, present, and future. In *Chapter 3 of Scientific Assessment of Ozone Depletion: 2018, Global Ozone Research and Monitoring Project–Report No. 58, World Meteorological Organization, Geneva, Switzerland.*

Checa-Garcia, R., Hegglin, M. I., Kinnison, D., Plummer, D. A., & Shine, K. P. (2018). Historical tropospheric and stratospheric ozone radiative forcing using the CMIP6 database. *Geophysical Research Letters*, *45*(7), 3264-3273. Retrieved from `https://agupubs.onlinelibrary.wiley.com/doi/abs/10.1002/2017GL076770` doi: 10.1002/2017GL076770

Fioletov, V. E., Bodeker, G. E., Miller, A. J., McPeters, R. D., & Stolarski, R. (2002). Global and zonal total ozone variations estimated from ground-based and satellite measurements: 1964–2000. *Journal of Geophysical Research: Atmospheres*, *107*(D22), ACH 21-1-ACH 21-14. Retrieved from `https://`

agupubs.onlinelibrary.wiley.com/doi/abs/10.1029/2001JD001350 doi: https://doi.org/10.1029/2001JD001350

Forster, P. M., Richardson, T., Maycock, A. C., Smith, C. J., Samset, B. H., Myhre, G., ... Schulz, M. (2016). Recommendations for diagnosing effective radiative forcing from climate models for CMIP6. *Journal of Geophysical Research: Atmospheres*, *121*(20), 12,460-12,475. Retrieved from https://agupubs.onlinelibrary.wiley.com/doi/abs/10.1002/2016JD025320 doi: 10.1002/2016JD025320

Frith, S. M., Kramarova, N. A., Stolarski, R. S., McPeters, R. D., Bhartia, P. K., & Labow, G. J. (2014). Recent changes in total column ozone based on the SBUV version 8.6 merged ozone data set. *Journal of Geophysical Research: Atmospheres*, *119*(16), 9735-9751. Retrieved from https://agupubs.onlinelibrary.wiley.com/doi/abs/10.1002/2014JD021889 doi: 10.1002/2014JD021889

Langematz, U., Schmidt, F., Kunze, M., Bodeker, G. E., & Braesicke, P. (2016). Antarctic ozone depletion between 1960 and 1980 in observations and chemistry–climate model simulations. *Atmospheric Chemistry and Physics*, *16*(24), 15619–15627. Retrieved from https://acp.copernicus.org/articles/16/15619/2016/ doi: 10.5194/acp-16-15619-2016

Langematz, U., Tully, M., Calvo, N., Dameris, M., de Laat, A., Klekociuk, A., ... Young, P. (2018). Polar Stratospheric Ozone: Past, Present, and Future. In *Chapter 4 of Scientific Assessment of Ozone Depletion: 2018, Global Ozone Research and Monitoring Project–Report No. 58, World Meteorological Organization, Geneva, Switzerland.*

Mastrandrea, M., Mach, K., Plattner, G.-K., Edenhofer, O., Stocker, T. F., Field, C. B., ... Matschoss, P. R. (2011). The IPCC AR5 guidance note on consistent treatment of uncertainties: a common approach across the working groups. *Climatic Change*, *108*, 675. Retrieved from https://doi.org/10.1007/s10584-011-0178-6

Morgenstern, O. (2021). The Southern Annular Mode in 6th Coupled Model Intercomparison Project models. *Journal of Geophysical Research: Atmospheres*, *126*(5), e2020JD034161. Retrieved from https://agupubs.onlinelibrary.wiley.com/doi/abs/10.1029/2020JD034161 (e2020JD034161 2020JD034161) doi: https://doi.org/10.1029/2020JD034161

Morgenstern, O., O'Connor, F. M., Johnson, B. T., Zeng, G., Mulcahy, J. P., Williams, J., ... Kinnison, D. E. (2020). Reappraisal of the climate impacts of ozone-depleting substances. *Geophysical Research Letters*, *47*(20), e2020GL088295. Retrieved from https://agupubs.onlinelibrary.wiley.com/doi/abs/10.1029/2020GL088295 (e2020GL088295 10.1029/2020GL088295) doi: https://doi.org/10.1029/2020GL088295

Myhre, G., Shindell, D., Bréon, F.-M., Collins, W., Fuglestvedt, J., Huang, J., ... Zhang, H. (2013). Anthropogenic and Natural Radiative Forcing. In *Climate Change 2013 - The Physical Science Basis* (chap. 8). Geneva, Switzerland: Intergovernmental Panel on Climate Change (IPCC). Retrieved from https://www.ipcc.ch/site/assets/uploads/2018/02/WG1AR5_Chapter08_FINAL.pdf

Newman, P. A., Daniel, J. S., Waugh, D. W., & Nash, E. R. (2007). A new formulation of equivalent effective stratospheric chlorine (eesc). *Atmospheric Chemistry and Physics*, *7*(17), 4537–4552. Retrieved from https://acp.copernicus.org/articles/7/4537/2007/ doi: 10.5194/acp-7-4537-2007

Riahi, K., van Vuuren, D. P., Kriegler, E., Edmonds, J., O'Neill, B. C., Fujimori, S., ... Tavoni, M. (2017). The Shared Socioeconomic Pathways and their energy, land use, and greenhouse gas emissions implications: An overview. *Global Environmental Change*, *42*, 153-168. Retrieved from https://www.sciencedirect.com/science/article/pii/S0959378016300681 doi:

https://doi.org/10.1016/j.gloenvcha.2016.05.009

Shindell, D., Faluvegi, G., Nazarenko, L., Bowman, K., Lamarque, J.-F., Voulgarakis, A., ... Ruedy, R. (2013). Attribution of historical ozone forcing to anthropogenic emissions. *Nature Climate Change*, *3*, 567. Retrieved from https://www.nature.com/articles/nclimate1835

Søvde, O. A., Hoyle, C. R., Myhre, G., & Isaksen, I. S. A. (2011). The HNO_3 forming branch of the HO_2 + NO reaction: pre-industrial-to-present trends in atmospheric species and radiative forcings. *Atmospheric Chemistry and Physics*, *11*, 8929–8943. Retrieved from https://doi.org/10.5194/acp-11-8929-2011 doi: 10.5194/acp-11-8929-2011

Stolarski, R. S., & Frith, S. M. (2006). Search for evidence of trend slow-down in the long-term TOMS/SBUV10:50 am 21/07/2021 total ozone data record: the importance of instrument drift uncertainty. *Atmospheric Chemistry and Physics*, *6*(12), 4057–4065. Retrieved from https://acp.copernicus.org/articles/6/4057/2006/ doi: 10.5194/acp-6-4057-2006

van der A, R. J., Allaart, M. A. F., & Eskes, H. J. (2015). Extended and refined multi sensor reanalysis of total ozone for the period 1970–2012. *Atmospheric Measurement Techniques*, *8*, 3021–3035. Retrieved from https://doi.org/10.5194/amt-8-3021-2015

Weber, M., Coldewey-Egbers, M., Fioletov, V. E., Frith, S. M., Wild, J. D., Burrows, J. P., ... Loyola, D. (2018). Total ozone trends from 1979 to 2016 derived from five merged observational datasets – the emergence into ozone recovery. *Atmospheric Chemistry and Physics*, *18*, 2097–2117. Retrieved from https://doi.org/10.5194/acp-18-2097-2018

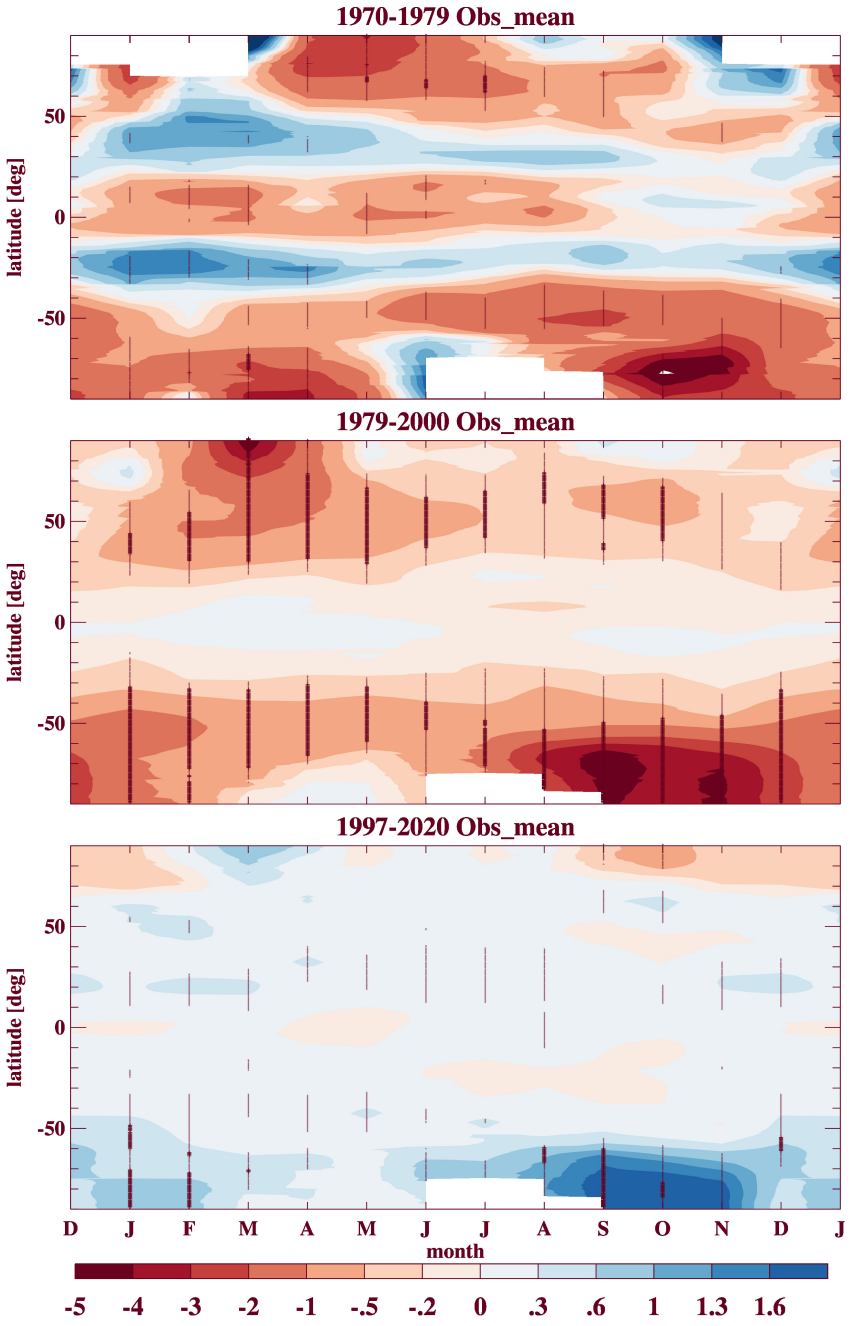

Figure 1. Trends in TCO (DU a^{-1}) in the observational-mean TCO dataset as functions of latitude and month of the year, for (top) 1970-1979, (center) 1979-2000 and (bottom) 1997-2020. Thin lines indicate that trends are significant at 84% confidence, thick lines at 97.5%. Here uncertainty accounts for both the trend uncertainty and any inconsistency across four datasets (excluding NIWA-BS 3.5.1; equation 1). Top two panels: nodes in 1970, 1979, 2000, and 2020. Bottom panel: nodes in 1970, 1979, 1997, and 2020.

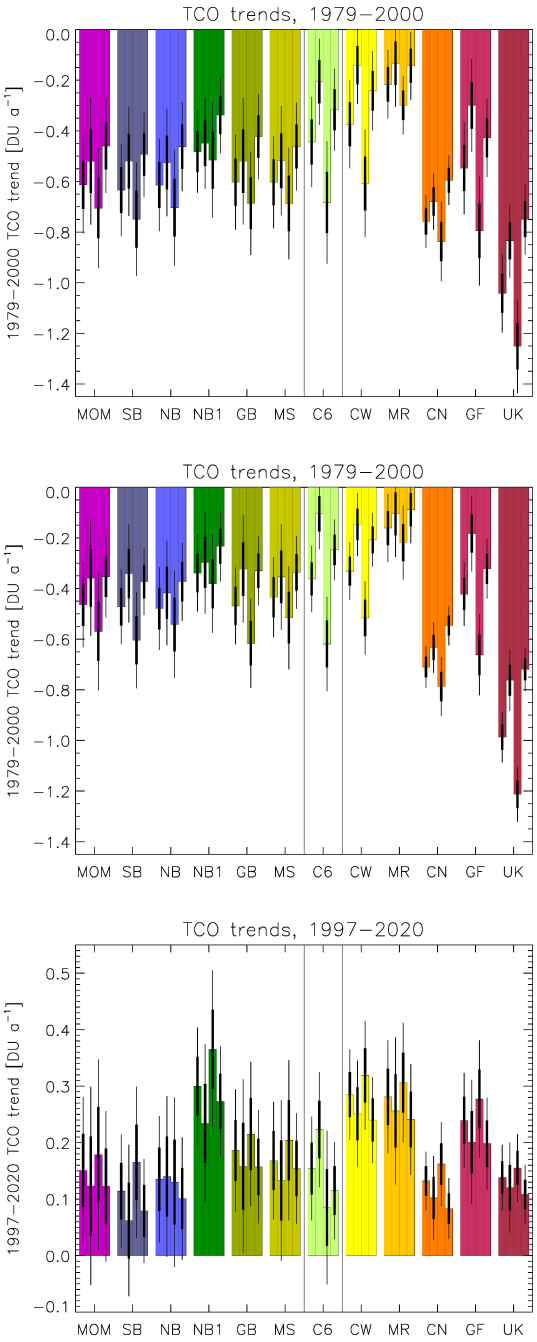

Figure 2. Global and regional TCO trends (DU a^{-1}). For each category, the four bars represent (left to right) global, Northern Hemisphere, Southern Hemisphere, and 60°S to 60°N means. The thick (thin) black bars denote the 68% (95%) confidence ranges for these trends. Top: 1979-2000, using simple linear regression. Center: 1979-2000, using three-node piewise linear regression with nodes in 1979, 2000, and 2020. Bottom: 1997-2020, with nodes in 1970, 1979, 1997, and 2020. SB = SBUV v86. NB = NIWA-BS. NB1 = NIWA-BS v3.5.1. GB = WOUDC ground-based. MS = MSR-2. C6 = CMIP6 ozone forcing dataset (Checa-Garcia et al., 2018). CW = CESM2-WACCM. MR = MRI-ESM2. CN = CNRM-ESM2-1. GF = GFDL-ESM4. UK = UKESM1-0-LL. The MOM is calculated based on the SB, NB, GB, and MS datasets, excluding NB1.

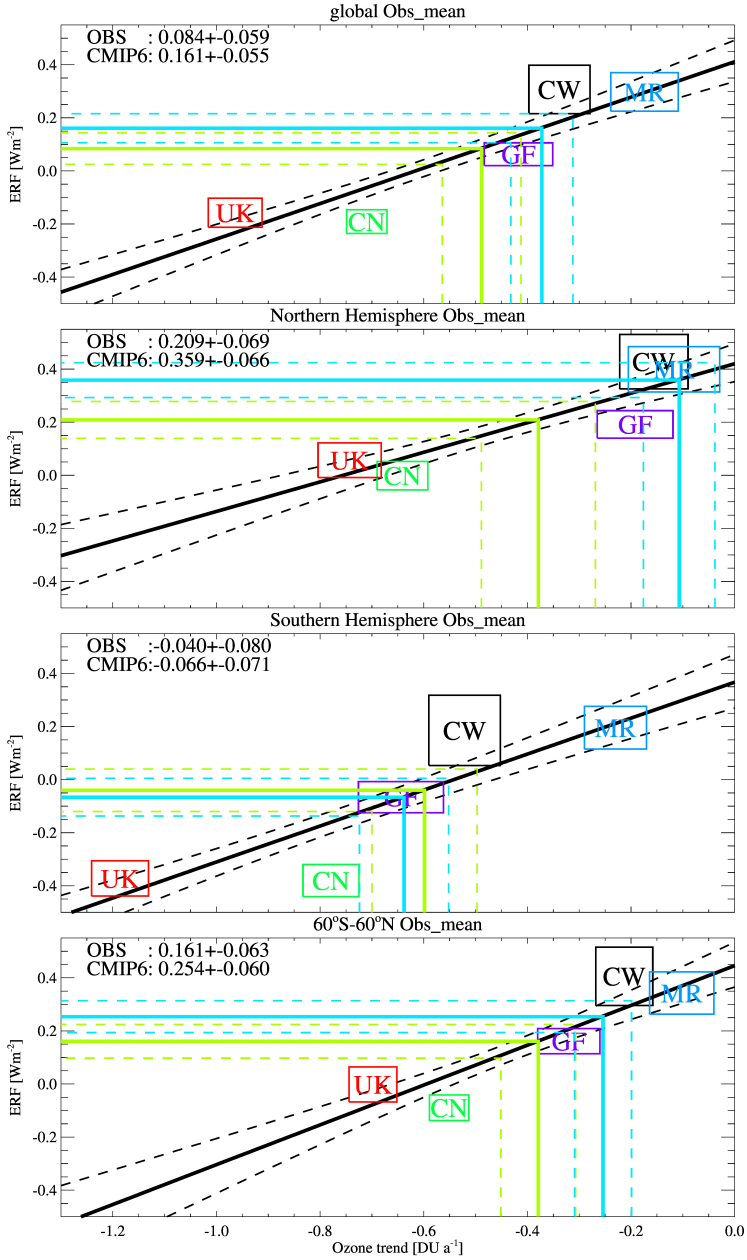

Figure 3. Colored rectangles: area-mean ozone trend for 1979–2000 and ERF of ODSs (accounting for all feedbacks) simulated by the five CMIP6 models. The width and height of the rectangles represent the statistical uncertainties of these quantities at the one-standard deviation or 68% confidence level. Black lines: least-squares linear fit (solid) with associated 68% confidence uncertainties (dashed). Green lines: estimated observational ozone depletion (solid) with its 68% confidence uncertainty (dashed) derived from the mean of the MSR-2, NIWA-BS v3.4, SBUV v86, and WOUDC ground-based climatologies, and the corresponding projection onto the ERF of ODSs. Light blue lines: the same but for the CMIP6 ozone climatology. The four panels represent the global, Northern-Hemisphere, Southern-Hemisphere, and 60°S to 60°N means for ozone depletion and the ERF. The labels in the top left corners of the panels represent the ERF of ODSs consistent with the EC calculation for the observations ("OBS") and the CMIP6 climatology ("CMIP6"). CN = CNRM-ESM2-1; CW = CESM2-WACCM; GF = GFDL-ESM4; MR = MRI-ESM2-0; UK = UKESM1-0-LL. Note that the inflection points for the uncertainty bounds (dashed green and blue lines) are located slightly off the EC (thick black line), a result of combining the uncertainty in ozone depletion with that in the EC. Updated after Morgenstern et al. (2020).